24th International Conference on Renewable Energies and Power Quality (ICREPQ'26)
Santander (Spain), 10th to 12th June 2026
ISBN-13: 978-84-09-82044-3

Impact of re-synchronization strategies on the power sharing of grid-forming converters at black start

J. Rodriguez-Gongora[1], A. Ordono[2], M. González-Pérez[2], M. Zubiaga[1], A. Sanchez-Ruiz[3]

[1] Department of Electronic Technology
Engineering School of Gipuzkoa, University of the Basque Country (UPV/EHU)
Avda. Otaola, 29, 20600 Eibar (Spain). E-mail: javier.rodriguezg@ehu.eus

[2] Department of Electrical Engineering
Engineering School of Gipuzkoa, University of the Basque Country (UPV/EHU)
Avda. Otaola, 29, 20600 Eibar (Spain)

[3] Department of Electronic Technology
Engineering School of Vitoria-Gasteiz, University of the Basque Country (UPV/EHU)
Nieves Cano 12, 01006 Vitoria-Gasteiz (Spain)

Abstract. Grid-forming (GFM) converters enable black start (BS) operation in converter-dominated power systems, where independently energized islands must be re-synchronized before interconnection. While re-synchronization is essential for stable reconnection, its impact on the power-sharing capability of GFM converters is not yet fully understood. This paper investigates how different re-synchronization algorithms affect active and reactive power sharing following island interconnection during BS. Time-domain simulations show that misalignment of internal control states and reference variables can lead to persistent power-sharing differences. In contrast, properly designed re-synchronization strategies minimize power sharing unbalances. The results highlight the importance of re-synchronization design for robust power sharing in converter-based BS applications.

Key words. Black start (BS), grid-forming (GFM), power sharing, re-synchronization.

1. Introduction

The increasing penetration of power electronic interfaced generation has transformed the dynamic behaviour of modern power systems. In particular, grid-forming (GFM) converters are emerging as a key enabling technology for future low-inertia grids, as they are capable of establishing voltage and frequency without relying on an external reference **[1]**. This capability makes GFM converters especially attractive for black start (BS) applications, where system restoration must begin from a de-energized network in the absence of a stiff grid **[2]**.

During BS, multiple islands may be energized independently and later reconnected as the restoration progresses **[3]**. A critical stage in this process is re-synchronization, during which voltage magnitude, frequency, and phase angle differences among islands must be reduced to acceptable limits prior to reconnection.

Re-synchronization algorithms introduce transient adjustments in the internal states of GFM converters, including frequency references, virtual rotor dynamics, and voltage setpoints. In contrast to conventional synchronous-machine-based systems, where mechanical inertia and damping contribute to natural power redistribution, converter-dominated systems rely entirely on control actions, making power sharing more sensitive to re-synchronization design choices.

Despite the critical role of power sharing for secure and efficient system restoration, the interaction between re-synchronization algorithms and steady-state and dynamic power-sharing performance has received limited attention in the literature. Some studies have proposed novel re-synchronization strategies and verified their power-sharing capability **[4], [5]**. However, no general theoretical analysis has been addressed. Furthermore, most analyses stick to linear droops, leaving out of the scope the effect on a general non-linear droop curve.

This article analyses the influence of re-synchronization algorithms on the power-sharing capability of GFM converters during BS operations. Particular attention is given to the evolution of active and reactive power sharing following interconnection, and power imbalances induced during and after re-synchronization. Through analytical assessment and time-domain simulations, the study highlights how different algorithms affect post-reconnection power sharing. It also provides insights for the design of re-synchronization strategies that preserve power-sharing characteristics of GFM schemes.

The work is structured as follows. Section 2 provides a description of the BS scenario and the fundamentals of GFM synchronization control. Section 3 describes the parametrization of generalized droop curves. Section 4 explains the influence of the re-synchronization algorithm on the GFM droop curve. Section 5 focuses on the validation of the theoretical analysis through simulation. Finally, Section 6 concludes the paper.

2. Black Start scenario and GFM control

The scenario at BS corresponds neither to a standalone nor to a grid-connected application. During the first stages of BS, GFM units with BS functionality work in standalone mode to energize the corresponding grid sector. In this step, the cranking paths, i.e. the lines and substations that need to be energized for a second generator to start, have the highest priority for energization **[6]**. Once a second generator has been powered up, the GFM must work in parallel with it in a coordinate way to pick up loads **[7]**. Finally, as the last step of BS, the islanded grid sector must re-synchronize with other restored portions of the grid to unify the power system **[3]**.

The nature of the second generator, whether a synchronous generator (SG), GFM or grid following (GFL) unit, defines the characteristics of the scenario. If GFM or SG, the scenario would be equivalent to a grid-connected scenario, where several voltage sources coexist. If GFL, however, the scenario would correspond to an islanded operation with some generation units, but a single voltage source. Regardless of the scenario, if more than one generator coexists, a coordinated response to load variations and their synchronization is essential.

In GFMs, the most extended approach for synchronization and load-sharing is droop control **[8]**. GFL units, on the other hand, may include droop control for grid support purposes, while their synchronization relies on a PLL **[9].**

Droop control is analogous to SG speed control: the injected power increases as speed falls below the reference value. Its equations for both the active and reactive power are given by (1) and (2), where P, Q, ω and E stand for the active and reactive power, and the frequency and voltage, respectively. Frequency and voltage are measured values in GFL, and internal values in GFM units. Superscript * indicates setpoint values, and m_ω, m_V denote droop coefficients.

$$P = P^* - m_\omega \cdot (\omega^* - \omega) \tag{1}$$

$$Q = Q^* - m_V \cdot (E^* - E) \tag{2}$$

In GFM units, the droop control is usually complemented with inertia emulation algorithms such as virtual synchronous generator (VSG). The inertia helps slowing down the frequency dynamics due to unbalances. As for reactive power droop, a low-pass filter is commonly added to filter power measurement noise and limiting its bandwidth.

3. GFM droop curves parametrization

Although the most extended droop curves correspond to linear droop, whose mathematical expressions have been summarized in (1) and (2), non-linear droop curves have also been proposed in literature to enhance the performance: piecewise droop, quadratic droop and exponential droop (a.k.a. "droop-e" **[10]**), among others. Figure 1 provides a visual comparison. In non-linear curves, droop coefficient (m_ω) is the first derivative of the droop curve, i.e. the slope.

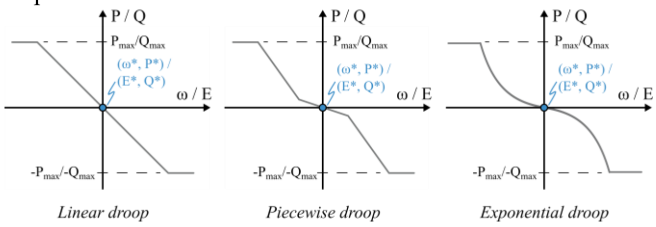

Fig.1. Linear, piecewise and exponential droop curves.

The motivation of these modified curves is to reduce the droop value near the rated frequency and voltage and increase it under excursions. This might be especially interesting for battery-based GFMs, where available headroom is critical, maintaining island stability while delegating frequency regulation in other generators during nominal operation. Note that droop with deadband, commonly used in GFL, is a particular case of the piecewise droop curve, where the slope in the deadband is zero, i.e. $m_\omega = 0$.

The parametrization of these curves depends on two main parameters, i.e. the reactive/active power setpoint (Q^*, P^*) and voltage/frequency setpoint (E^*, ω^*), and on the shape of the curve itself. As for the linear curves, i.e. the linear and piecewise droops, only the droop coefficient of each interval should be set. Regarding the exponential droop, two parameters (α, β) need to be adjusted, as shown in (3). These are selected according to the minimum droop value, i.e. when $(\omega - \omega^*) = 0$, and its maximum value when $P = \pm P_{max}$.

$$P = P^* - sign(\omega - \omega^*) \cdot \alpha \cdot \left(e^{\beta \cdot |\omega - \omega^*|} - 1\right) \tag{3}$$

4. Re-synchronization algorithm: influence on the GFM droop curve

As mentioned in Section 2, the final step of the BS corresponds to the re-synchronization of the power islands. Figure 2 shows this scenario. Each island, denoted by the subindex $i \in [1,2]$, can be represented as an equivalent voltage source (E_i), representing the GFM(s) and other generators (GFL or SG), and a parallel impedance ($Z_{load,i}$) to account for the loads. The series impedance of the line between the two islands (Z_i) is also included.

To resynchronize two asynchronous power grids (in this case, grid 2 to grid 1), voltage amplitude, frequency and phase at both sides of the breaker in-between must match each other. To achieve this, conventional secondary control methods based on slow PI controllers can be used **[11]**, as shown in Figure 3. It is worth mentioning that, since the frequency and phase are dependent on one another, a unique phase PI can synchronize both.

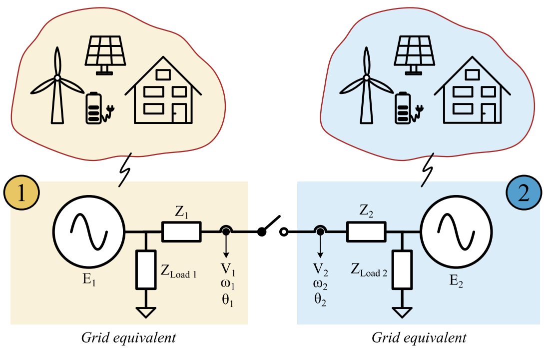

Fig.2. Equivalent circuit of the power system prior to re-synchronization.

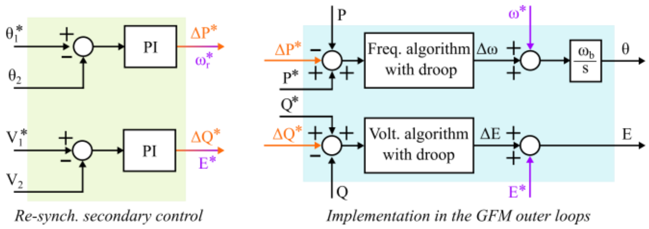

Fig.3. Re-synchronization control algorithm and implementation.

The input of the controllers are the phase and voltage errors at the point of interconnection. However, since angles are normally wrapped between 0 and 2π , phase PI needs a slight modification. $\theta_1 - \theta_2$ may at some instants change abruptly when the integration is wrapped. This generates spikes in the angle error, which compromise the behaviour of the re-synchronization control. To solve this, a rate limiter can be used to average the angle error **[11]**. An alternative approach is to suppress the wrapping of the angles when re-synchronization is enabled.

The output of the PIs can be either added to the power, as in **[11]**, or to the frequency and voltage setpoints, as in **[4]**. The philosophy behind each one is different and, in some cases, can affect the system dynamics and stability, as will be discussed in this section. For the sake of generalization, a non-linear droop curve will be used. Note that for pure linear droop, the modification of the power setpoints or the voltage/frequency setpoints are equivalent to each other, due to the translation invariance of a line in a 2D plane.

A. Voltage and frequency setpoints modification

Modifying the voltage and frequency is translated into a horizontal translation of the droop curve, as depicted in Figure 4. The frequency and voltage of grid 1, used as references for the PIs, are marked with a purple vertical line, while the frequency/voltage setpoints of grid 2 are superposed to the y-axis.

The translation of the droop curve depends on the operating point of grid 2. If working at nominal conditions (pink point), the new droop curve will settle at exactly the voltage/frequency setpoints of grid 1 (red curve). However, if working initially out of the origin (blue point), the error between the voltage/frequency setpoint and the true voltage/frequency of grid 2, denoted as δ , needs to be compensated by the PIs for the new operation point to be at ω_1 and E_1 . Thus, the resulting droop curve (orange curve) is further right and centred at $\omega_1/E_1 + \delta$.

It should be noted that the resulting droop value is not the same in both cases. The minimum droop value is associated to the red curve and the pink point, while a higher droop value is associated to the orange curve and the blue point. In any case, the droop value of the initial operating point in grid 2 is maintained during and at the instant of re-synchronization.

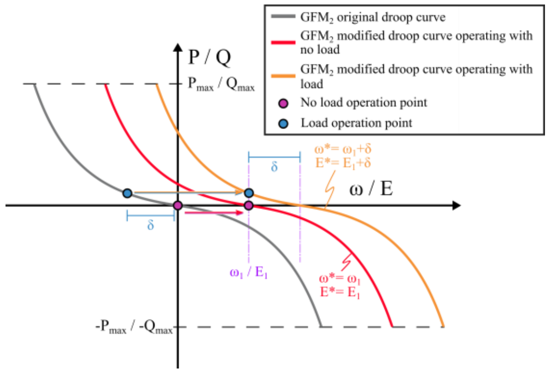

Fig.4. Effect of voltage/frequency setpoint modification on the droop curve.

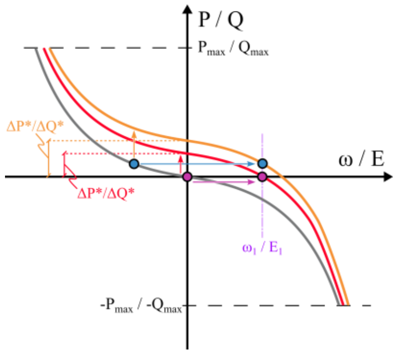

Fig.5. Effect of power setpoint modification on the droop curve.

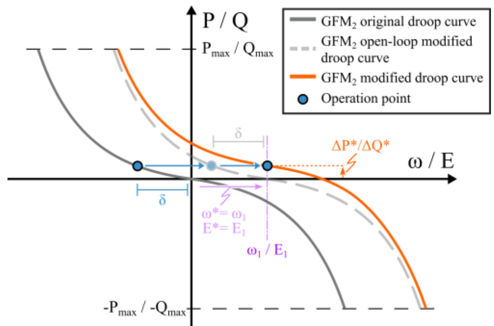

Fig.6. Effect of hybrid modification on the droop curve.

B. Power setpoints modification

The modification of the power setpoints is associated with a vertical translation of the droop curve, as depicted in Figure 5. Depending on the initial operating point of grid 2, the modified droop curve changes its offset, as illustrated by the pink and blue points and the red and orange curves, respectively. Nevertheless, the droop (slope) at the new operating point at ω_1 and E_1 remains invariant. It only depends on two factors: 1) the horizontal distance between the voltage/frequency setpoint of grid 2 and the voltage/frequency setpoint of grid 1, i.e. $\omega_1 - \omega_2$ and $E_1 - E_2$, and 2) the mathematical expression of the non-linear droop curve.

The underlying philosophy of this implementation could be thought of as "make grid 1 follow grid 2 conditions". As the droop curves are kept centred at grid 2 voltage/frequency setpoints, the resulting operating point after resynchronization is characterized by a higher droop, as in the case of a voltage/frequency excursion. This makes grid 2 more sensitive to voltage/frequency variations and react more aggressively, compromising load sharing capability and needing higher power reserves to respond to load changes **[12]**.

C. *Hybrid modification*

Another novel proposal consists of modifying both the frequency/voltage setpoint and the power setpoint. This implementation admits multiple combinations and hybridization methods, e.g. dividing the PI output into two terms by means of weight factors or changing one of the two setpoints in open loop and applying the PI output to the other to compensate for the open-loop error. However, for the sake of conciseness, only the latter option will be described in this subsection.

Opposite to the philosophy described in the previous subsection, the philosophy "make grid 2 follow grid 1 conditions" could also be applied. For that, sticking to grid 1 voltage/frequency setpoints is required (i.e. $\boldsymbol{\omega_2^*} = \boldsymbol{\omega_1}$ and $\boldsymbol{E_2^*} = \boldsymbol{E_1}$), which may lead to a steady state error depending on the initial operating point of grid 2, as was shown in Figure 4. To compensate for that error, the power setpoint can be modified with the PI output, i.e. the droop curve can be translated vertically. This corresponds to a hybrid case, where the voltage/frequency setpoint is adjusted in open loop, and the PI output modifies the power setpoint to cancel the steady state error.

Figure 6 depicts the resulting modification of the droop curve. Here, it can be appreciated that this modification corresponds to a diagonal translation of the droop curve. With this transformation, the new operating point is modified and set to the minimum droop value. In essence, this implementation moves the centre of the droop curve to the operating point needed for re-synchronization. This way, the whole system will operate around the voltage/frequency of grid 1 after re-synchronization. This implementation may be suitable when the power island is connected back to the main grid or to a much larger restored grid section, where the generators of the power island are unable to modify substantially the operating point of the whole system.

5. Test case scenario and results

To validate the previous theoretical analysis, a simplified version of the scenario of Figure 2 has been used (see Figure 7). The local loads of GFM_1 have been removed, an external common load (Z_B) with breaker (S_B) has been added and the nomenclature of GFM_2 local loads with breaker has been modified (Z_A and S_A).

For the sake of simplicity, the simulation will focus only on the active power sharing. Therefore, re-synchronization voltage PI and GFM voltage regulation algorithm will be left out of the scope of the analysis.

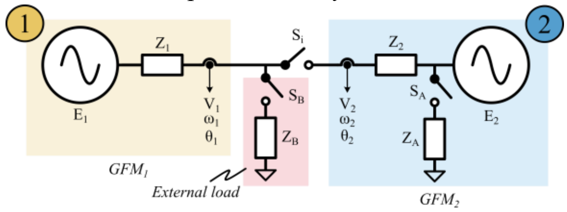

Fig.7. Simplified re-synchronization scenario for simulation.

A. *Parametrization*

The simulation is composed of three steps: 1) the re-synchronization of GFM_2 to GFM_1, 2) the response to a decrease in the load and 3) the response to an increase in the load.

The sequence of events is as follows: at 0.1 s the local load of GFM_2 ($P = 0.5\,pu$) is connected by closing S_A. At 0.15 s, re-synchronization is enabled and finishes with the closing of S_i once the phase and voltage RMS errors over a 0.2 s time window are below 2%. When already re-synchronized, at 2.2 s the active power of the loads is reduced by opening S_A. Then, at 2.8 s the active power of the loads is increased by closing S_B and connecting Z_B ($P = 1.16\,pu$).

Regarding the parametrization of the GFMs, GFM_1 has a linear active power droop while GFM_2 has an exponential one. The frequency setpoints are set initially to $\omega_1^* = 1.005\,pu$ and $\omega_2^* = 1\,pu$ respectively. The values of the parameters of the scenario are summarized in Table I.

It is worth noting that different PI gains have been used for the three strategies in order to make the re-synchronization occur within the simulation time window.

Table I. Parametrization of the simulation scenario.

	Parameter	Value
Base values	Base voltage (V_b)	33 kV
	Base power (S_b)	157.56 MVA
	Base frequency (f_b)	50 Hz
GFM 1	Line impedance (Z_1)	0.0126 + j0.3 pu
	Linear droop (m_ω)	50.34 pu
	Inertia (H)	1 s
GFM 2	Line impedance (Z_2)	0.0126 + j0.3 pu
	Exponential droop (α)	0.5
	Exponential droop (β)	100
	Exponential droop (D_{min})	50 pu
	Inertia (H)	1 s
Re-synch. PI	Phase PI (k_p)	0.1 / 1 / 1
	Phase PI (k_i)	3 / 5 / 5

B. *Simulation results*

The simulation results of each one of the strategies explained in Section 4 are shown in the columns of Figure 8. In the upper part, the droop curves and the respective operation points for the power decrease at 2.2 s (denoted as "a-A") and the increase at 2.8 s (denoted as "b-B"). In the lower part of the figure, the simulation time-domain results of active power, frequency and phase difference are also included.

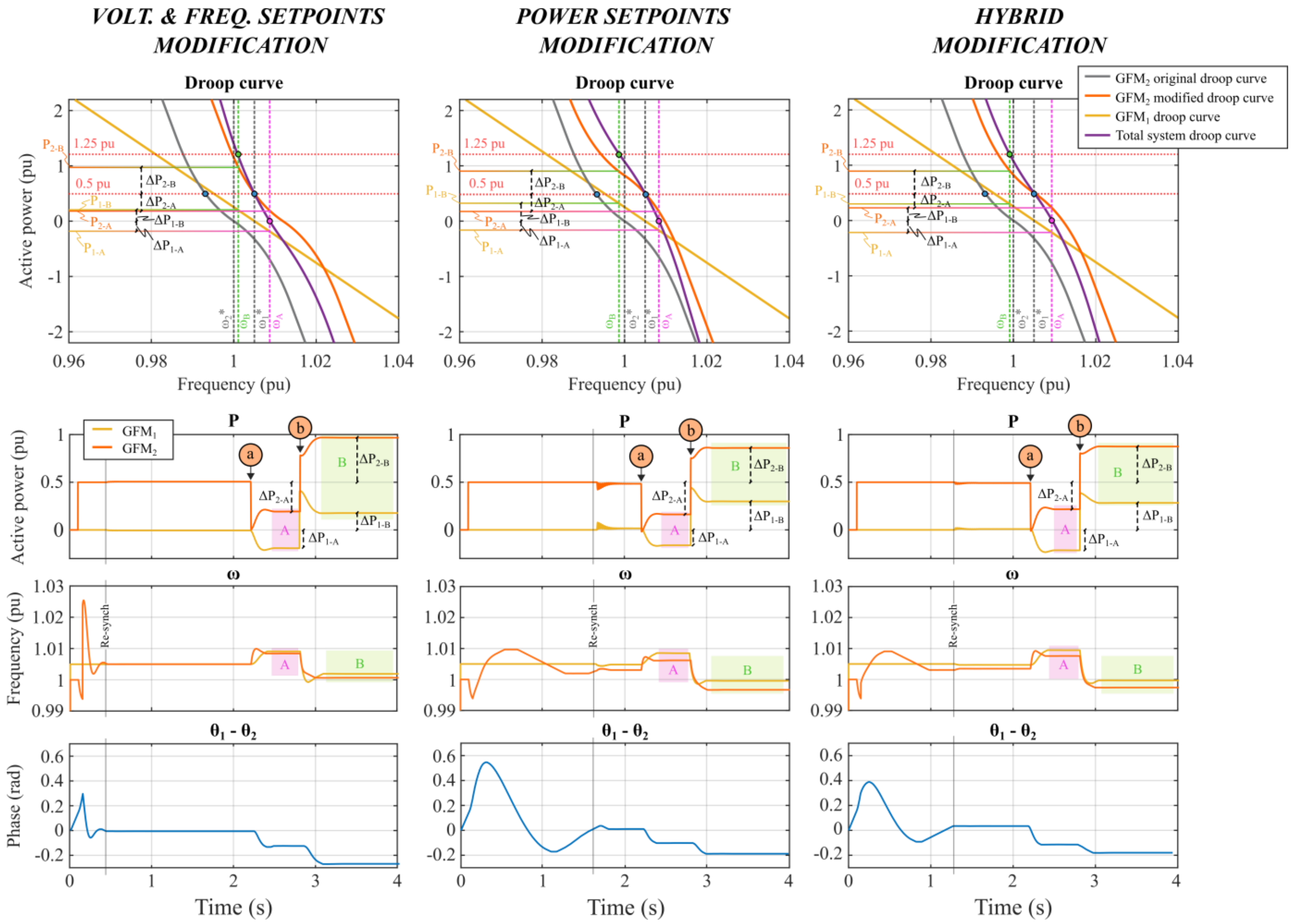

Fig.8. Simulation results of the *volt. & freq. setpoints, power setpoints* and *hybrid modifications* face to power decrease and increase perturbations.

To validate the theoretical analysis of Section 4, the total system droop curve has been obtained and plotted in the upper subplots of Figure 8. This curve is the sum of the individual droop curves of GFM_1 and GFM_2 and determines the operation point of the whole system (i.e. frequency and power share) according to the active power of the load. The green and pink points correspond to the operation points after perturbations "a-A" and "b-B", respectively. The power share at these points has also been depicted by the horizontal lines of P_{1-A}, P_{2-A} , P_{1-B} and P_{2-B} . Note that, since GFM_2 resynchronizes while supplying 0.5 pu to the local loads and GFM_1's output power is zero, the response to the power perturbations "a-A" and "b-B" (denoted as ΔP) needs to be measured from this initial operation point with $P_{GFM1} = 0$ and $P_{GFM2} = 0.5\,pu$.

Comparing the upper droop plots with the time-domain active power results, the match between the theoretical and simulation power response to the power perturbations is evidenced. A more exhaustive analysis reveals that the power sharing is affected by the re-synchronization strategy used.

In terms of power decrease sharing (perturbation "a-A"), the *power setpoints modification* exhibits the greatest power variation ($\Delta P_{2-A} = -0.34\,pu$), due to the higher droop face to perturbations that move the frequency away from GFM_2 setpoint, associated with the philosophy "make grid 1 follow grid 2". *Hybrid modification*, on the other hand, as synchronized with the same frequency setpoint as GFM1, shows the lowest power variation according to the non-linear droop curve ($\Delta P_{2-A} = -0.28\,pu$). The *volt. & freq. setpoints modification* shows an intermediate value ($\Delta P_{2-A} = -0.31\,pu$), as the perturbation moves the frequency closer to the centre of the droop curve (further right) decreasing the slope. It is worth mentioning that if the grid to which GFM_2 is connected is a stiff grid, the *power setpoint modification* may not be adequate, since both power sharing capability and GFM_2 energy resource duration could be endangered.

Regarding the power increase sharing (perturbation "b-B"), following the same philosophy, the *power setpoints modification* presents the lowest variation ($\Delta P_{2-B} = 0.35\,pu$) since the perturbation moves the frequency closer to GFM_2 setpoint. The *volt. & freq. setpoints modification* shows in this case the highest power ($\Delta P_{2-B} = 0.47\,pu$) almost reaching the power limit. This is due to the extra horizontal displacement of the droop curve introduced by the PI compensation, which moves the centre of the curve further right. Since this perturbation tends to reduce the frequency (move to the left), GFM_2 operates in the steepest region of its droop, reacting aggressively to frequency reductions. As for the *hybrid modification*, an intermediate power response is observed ($\Delta P_{2-B} = 0.37\,pu$), characterized by an operation point in the middle region of the non-linear droop curve, below the steepest zone and above the centre region. In this case, it is worth noting that *volt. & freq. setpoints modification* may oppose or aid depending on the initial operation point of GFM_2 prior to re-synchronization, as the horizontal location of the curve is determined by the compensation term $\boldsymbol{\delta}$. If positive, the centre would be further right, as in Figure 8, but if negative, it can be on the left side, inverting thus the behaviour.

Finally, regarding the speed of the re-synchronization, the *volt. & freq. setpoints modification* shows a substantial reduction in the time needed for re-synchronization when compared to the other two strategies, due to the bypassing of the GFM outer loops dynamics. The next one is the *hybrid modification*, thanks to the feedforward of voltage and frequency setpoints in open loop, which help reduce the PI compensation bundle. As for the *power setpoints modification* the restricted dynamics of the GFM loops, worsen the re-synchronization speed.

6. Conclusions

This paper has analysed how the re-synchronization algorithms used in the last step of a BS affect the power sharing between GFM units. The theoretical analysis has provided insights regarding how each strategy modifies the droop curve of the GFM unit for a general non-linear case. This analysis has then been validated in simulation, where a comparative of these algorithms has been performed.

From the comparative, the *volt. & freq. setpoints modification* has shown the fastest re-synchronization time, while it has also shown the highest GFM_2 power variation face to load increase, which could compromise the stability of the GFM unit itself. Moreover, it has been shown that the droop characteristics are determined by the initial operating point prior to re-synchronization, which endangers robustness.

The *power setpoints modification* is based on the philosophy of "make GFM_1 follow GFM_2". As a result, the response perturbations that move the frequency away from GFM_2 setpoint is much more aggressive, making it suitable when connecting to weaker grids in which GFM_2 may determine the operating point of the system. Regarding the re-synchronization speed, this algorithm has the worst performance due to the dynamic limitation of GFM outer loops.

On the other hand, the *hybrid modification*, based on the "make GFM_2 follow GFM_1" principle, exhibits lower power variations face to disturbances, as is characteristic of the central region of the non-linear droop. This makes this algorithm useful when connecting to stronger grids, where the operating conditions are not substantially affected by the power injection of GFM_2. Additionally, in terms of re-synchronization speed, it outperforms the *power setpoints modification* thanks to the open-loop voltage and frequency setpoints feedforward.

Acknowledgement

This work has been supported in part by the European Partnership on Metrology (EURAMET), co-financed from European Union's Horizon Europe Research and Innovation Program and by the Participating States under Project 24GRD08 GridForm. This work has also been funded in part by the Basque Government within the research program ELKARTEK under project RESINET+ (KK-2025/00100), GISEL Research Group (IT1799-26) and E4GRID Research Group (IT1808-26).

References

[1] J. Matevosyan *et al.*, «Grid-Forming Inverters: Are They the Key for High Renewable Penetration?», *IEEE Power and Energy Mag.*, vol. 17, n.º 6, pp. 89-98, nov. 2019, doi: 10.1109/MPE.2019.2933072.

[2] Y. Du, H. Tu, X. Lu, J. Wang, y S. Lukic, «Black-Start and Service Restoration in Resilient Distribution Systems With Dynamic Microgrids», *IEEE J. Emerg. Sel. Topics Power Electron.*, vol. 10, n.º 4, pp. 3975-3986, ago. 2022, doi: 10.1109/JESTPE.2021.3071765.

[3] Y. Fan, N. Chen, Y. Zhao, X. Ding, R. Zhang, y X. Zhang, «Review of methodology and best practice of power system restoration plan», *Energy Internet*, vol. 1, n.º 2, pp. 123-140, nov. 2024, doi: 10.1049/ein2.12022.

[4] C.-T. Lee, R.-P. Jiang, y P.-T. Cheng, «A grid synchronization method for droop controlled distributed energy resources converters», en *2011 IEEE Energy Conversion Congress and Exposition*, Phoenix, AZ, USA: IEEE, sep. 2011, pp. 743-749. doi: 10.1109/ECCE.2011.6063844.

[5] D. Sharma, F. Sadeque, y B. Mirafzal, «Synchronization of Inverters in Grid Forming Mode», *IEEE Access*, vol. 10, pp. 41341-41351, 2022, doi: 10.1109/ACCESS.2022.3167521.

[6] K. Verclas, «he Black Box of Blackstart: Electricity Reliability and Interdependency Considerations for State Energy Offices».

[7] J. G. O'Brien *et al.*, «Electric Grid Blackstart: Trends, Challenges, and Opportunities».

[8] R. Rosso, X. Wang, M. Liserre, X. Lu, y S. Engelken, «Grid-Forming Converters: Control Approaches, Grid-Synchronization, and Future Trends—A Review», *IEEE Open J. Ind. Applicat.*, vol. 2, pp. 93-109, 2021, doi: 10.1109/OJIA.2021.3074028.

[9] Y. Zuo, Z. Yuan, F. Sossan, A. Zecchino, R. Cherkaoui, y M. Paolone, «Performance assessment of grid-forming and grid-following converter-interfaced battery energy storage systems on frequency regulation in low-inertia power grids», *Sustainable Energy, Grids and Networks*, vol. 27, p. 100496, sep. 2021, doi: 10.1016/j.segan.2021.100496.

[10] R. W. Kenyon, A. Sajadi, y B. M. Hodge, «Autonomous grid-forming inverter exponential droop control for improved frequency stability», *International Journal of Electrical Power & Energy Systems*, vol. 172, p. 111160, nov. 2025, doi: 10.1016/j.ijepes.2025.111160.

[11] A. Alassi, K. Ahmed, A. Egea-Alvarez, y C. Foote, «Modified Grid-forming Converter Control for Black-Start and Grid-Synchronization Applications», en *2021 56th International Universities Power Engineering Conference (UPEC)*, Middlesbrough, United Kingdom: IEEE, ago. 2021, pp. 1-5. doi: 10.1109/UPEC50034.2021.9548162.

[12] A. Ordono, A. Sanchez-Ruiz, M. Zubiaga, F. J. Asensio, y J. Rodriguez-Gongora, «Overload Mitigation of Inertial Grid-Forming Inverters Under Frequency Excursions», *Applied Sciences*, vol. 15, n.º 10, p. 5316, may 2025, doi: 10.3390/app15105316.